Carbonates Evaporites (2017) 32:415–430
DOI 10.1007/s13146-017-0356-3

REVIEW ARTICLE

Stable isotope and aquatic geochemistry of a typical subtropical karst subterranean stream in southwest China

Tao Zhang[1,2] · Junbing Pu[2] · Jianhong Li[2] · Daoxian Yuan[1,2] · Li Li[1,2]

Accepted: 25 April 2017 / Published online: 16 May 2017

Abstract A hydrogeochemical and isotopic study was conducted on the subterranean karst stream, namely the Guancun subterranean stream (GSS). The hydrogeochemical processes of the GSS were controlled through calcite dissolution and precipitation and were driven by the concentration of CO_2, which controlled changes in the pH and of PCO_2 in the water. The $\delta^{18}O$ and δD values of the GSS were within the global meteoric water line and the local meteoric water line, thereby indicating that the water of the GSS comes from precipitation. Certain abnormal $\delta^{18}O$ and δD values suggest the effect of evaporation on the GSS given its use in a particular irrigation system, wherein the GSS in transformed into a surface stream and flows for a relatively long time on the surface during the wet season. The $\delta^{13}C_{DIC}$ values of the GSS range from −13.5 to −11.3‰ in the dry season and from −13.9 to −9.5‰ in the wet season, thereby indicating that the GSS belongs to a semi-open system. The $\delta^{13}C_{DIC}$ values in the GSS were formed by the $\delta^{13}C_{DIC}$ values of the soil CO_2 and carbonate dissolution at different proportions. According to the simplified mass balance formula, the contributions of carbonate dissolution to the dissolved inorganic carbon (DIC) of the GSS were calculated to be 50.2–58.3% and 48.7–64.7% in the dry and wet seasons, respectively, thereby indicating a less than 50% carbonate dissolution contribution during the formation of DIC in karst groundwater. Moreover, sulfuric acid and nitric acid were observed to participate in karst processes.

Keywords Hydrogeochemistry · Stable isotopes · Carbonate dissolution · DIC · Subterranean karst stream

Introduction

China's southwestern region is the largest continuous karst area in the world and has an area of about 532,600 km^2, wherein local water resource development and utilization units target karst groundwater (Yuan 2000; Cao et al. 2004). However, the peculiar geographical and hydrogeological circumstances of the karst regions result in groundwater that is vulnerable to anthropogenic pollution that requires difficult and time-consuming rehabilitation projects once it is contaminated (Lang et al. 2006).

The regional evolution of the hydrogeochemical characteristics in karst groundwater systems and their coupled relationship with the geology and environment of the region are of great significance to development, utilization, and protection of underground river water resources (Pu 2011). Extensive research has been conducted on the topography and geological structure of karst aquifers, as well as the interactions of all of the components involved and their respective effects on the water chemistry of the aquifers (Gonfiantini and Zuppi 2003; Marfia et al. 2004; Sebela and Liu 2014). Moreover, the contaminant transport processes and mechanisms, and the hydrological dynamics of the underground water were explored (Lee and Kim 2007; Liu et al. 2007; Hu et al. 2015; Zhao et al. 2015). Likewise, tracer tests were conducted to trace the connections of the karst groundwater in karst aquifers (Yang

✉ Junbing Pu
junbingpu@karst.ac.cn

[1] Chongqing Key Laboratory of Karst Environment, School of Geographical Sciences, Southwest University, Chongqing 400715, China

[2] Key Laboratory of Karst Dynamics, Ministry of Land and Resources and Guangxi; Institute of Karst Geology, Chinese Academy of Geological Sciences, NO.50, Qixing Ave, Qixing District, Guilin 541004, China

2010). Recent studies have explored the hydrogeochemical processes that control the quality and chemical characteristics of karst groundwater in karst aquifers (Verbovšek and Kanduč 2016; Yuan et al. 2017). However, the hydrogeochemistry of karstic aquifers is often difficult to evaluate given the gross heterogeneities in its permeability, hydraulic conductivity, mixed conduits, and diffusive flow (Lang et al. 2006). Therefore, more case studies and data collection are necessary to better understand the hydrogeochemical characteristics of karst groundwater.

Karst groundwater hydrogeochemistry is mainly affected by natural aspects such as stratum, climate, soil, vegetation, and human activities, which include industrial and agricultural activities, urban expansion, and mining (Pu 2011), thereby complicating the analysis of the factors and processes involved. In addition, a karst subterranean stream lies within a relatively closed space, which complicates the collection of hydrogeochemical information within the aquifer's interior and challenges the identification of dominant hydrogeochemical processes in the karst subterranean streams.

Underground river outlets provide an in-depth understanding of the hydrogeochemical characteristics of karst subterranean streams (Liu et al. 1997; Peyraube et al. 2012). In addition, stable isotopes (H, O, and C) are useful in tracing and identifying the origin of groundwater, aquifer water flow, and the transformation process (Taniguchi et al. 2000; Kanduč et al. 2007; Han et al. 2010; Al-Charideh 2011; Tillman et al. 2014; Verbovšek and Kanduč 2016). Previous studies have employed a hydrochemical method to investigate sources of pollution (Lang et al. 2006) and to identify water–rock interaction in groundwater (Rao et al. 2009). However, few studies have combined hydrochemical and isotopic methods to analyze the hydrogeochemical processes present in karst groundwater (Pu 2011; Pu et al. 2013; Yuan et al. 2017).

The Guancun subterranean stream (GSS) is a typical karst underground river that is in an agricultural region and is the primary local source of drinking, irrigation, and residential water. However, GSS pollution has increased in recent years. In particular, nitrate and sulfate concentrations have noticeably increased within the past two decades (Guo et al. 2007). Local governments require the thorough understanding of GSS hydrogeochemical processes to generate appropriate karst groundwater protection policies. The present study investigated the predominant hydrogeochemical processes in the GSS using the seasonal variations of isotopic (O, H, C) and hydrochemical parameters to identify the origin of the groundwater, investigate the water/rock interactions, and determine the dominant hydrogeochemical processes in karst groundwater. The results of this study provide a scientific basis for protection and rational utilization of GSS groundwater resources.

Study area

The GSS is located in the town of Daliang, Rong'an County, Guangxi Zhuang autonomous Region, China. The GSS outlet is located at 109° 20′ 3.41″ E and 24° 52′ 5.34″ N at an altitude of 160 m (Fig. 1). The study area is dominated by a subtropical monsoon climate with an annual average temperature of 20 °C and has an annual average rainfall of 1726 mm. The study area has obvious dry seasons and wet seasons. The dry season extends from September to February, and the wet season extends from March to August and accounts for about 90% of the annual total rainfall.

The GSS system was developed in the carbonate rocks of the Rongxian formation (D_3r, Upper Devonian) (Fig. 1). Rainfall is the only recharge for groundwater in the GSS catchment area. The surface rivers are intermittent and are only filled with water during the wet season. Some discrete swallow holes, sinkholes, and karst windows are scattered within approximately 30.5 km^2 of the GSS catchment area. The depth of the water level in the karst windows ranges from 8 to 12 m below the ground level during the dry season, while the water rises above the ground surface in some depressions during the flood season, thereby submerging farmlands, roads, houses, and other objects. Water level seasonal fluctuations correspond to rainfall. The flood decline process generally occurs over a 1-week period, and a tracer test in the general conduit indicated that the average flow velocity was 726 m per day (Guo and Jiang 2009).

The GSS catchment is dominated by a typical karst peak-cluster with large karst dolines and sinkholes. The soil on the stone peaks is thin, but can be more than 2 m in some depressions such that the depressions become productive land for the local residents. The field area is 0.76 km^2 in area and is mainly distributed in a depression, which includes a paddy field, dry land, and a residential area, thereby accounting for only 2% of the total area. Paddy fields cover 0.58 km^2 and account for 76.5% of the total field area. The dry land plants are mainly sugar cane, corn, or vegetables. The vegetation in the catchment is composed of broad-leaved forest, shrub, pasture, and a small amount of economic forest. Therefore, C_3 plants are mainly distributed in the study area. C_3 plants refer to the C in CO_2, which is directly photosynthesized to phosphoglycerate in the plant. C_4 plants refer to the C in CO_2 that are first photosynthesized to oxaloacetic acid first and then to phosphoglycerate in the plant (Gong et al. 2009).

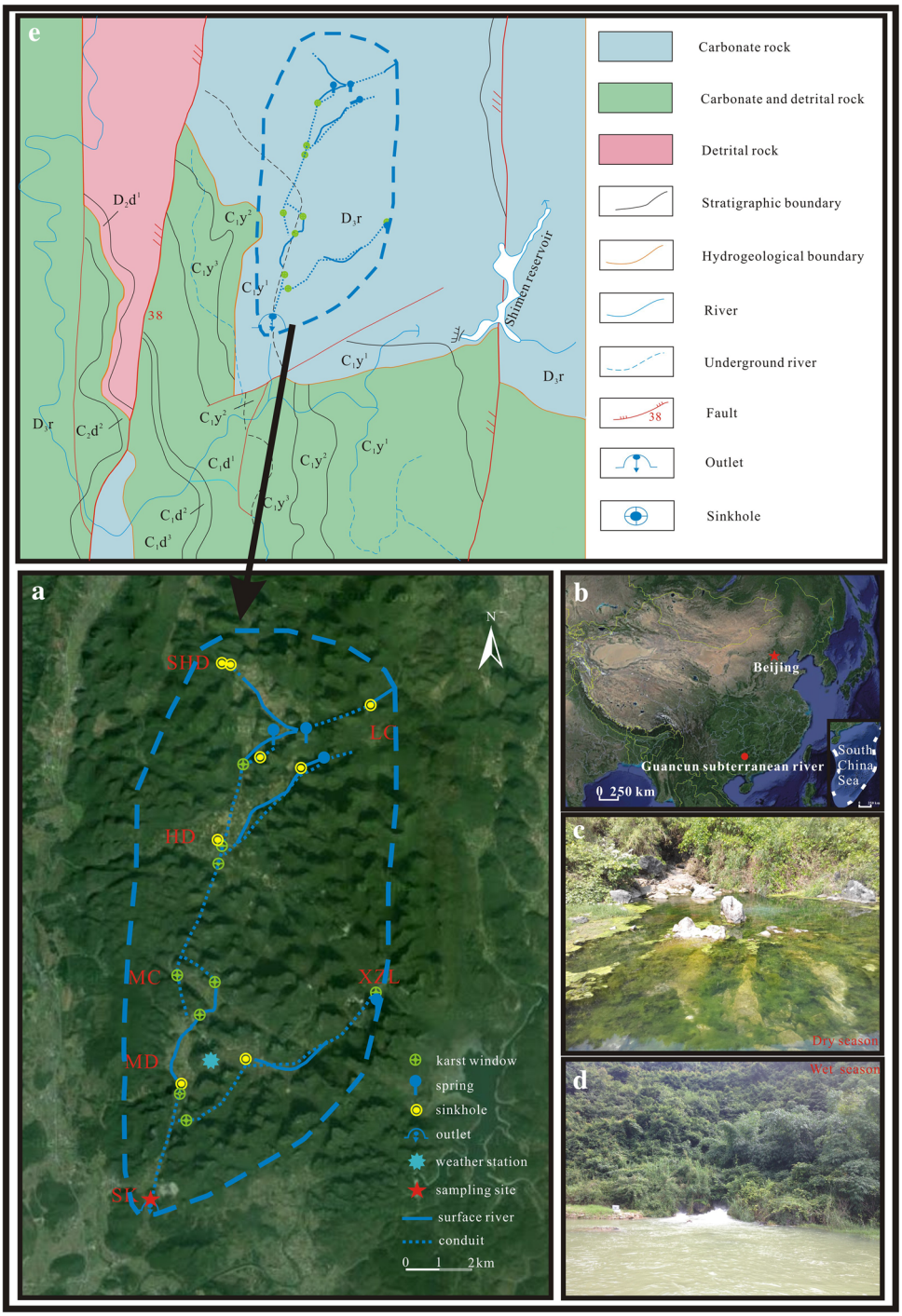

Fig. 1 Hydrogeological map of the study area: **a** distribution of the sampling location, **b** location map of the study area, **c** low discharge at the sampling site, **d** peak discharge at the sampling site, and **e** geological map of the study area

Groundwater sampling and analysis

A sampling campaign was conducted from September 2013 to September 2015 at the outlet of the GSS. The water temperature, pH, and specific conductivity (SpC, 25 °C) were measured in the field using a multiparameter probe (WTW 3430, WTW GmbH, Weilheim, Germany) under the following conditions: 0.1 °C, 0.004 pH unit, 1 µs/cm, and 0.1 mg/L. The total alkalinity of the water was titrated in the field using a portable alkalinity meter (Merck KGaA Co., Germany) with a precision of 0.05 mmol/L. Following water sample collection using injection syringes, the samples were immediately filtered through 0.45 µm-filter membranes for ion analyses and subsequently stored in 600 mL high-density polyethylene (HDPE) bottles. Water samples for cation determination were acidified to a pH < 2 using HNO_3. The samples used for the stable carbon isotope of the dissolved inorganic carbon ($\delta^{13}C_{DIC}$)

analysis were filtered into 15 mL HDPE bottles using 0.22 μm acetate rayon filters. These samples were immediately preserved using three drops of a saturated $HgCl_2$ solution to prevent microbial alteration. Oxygen and hydrogen isotopic analyses ($\delta^{18}O$ and δD) samples were collected in 30 mL HDPE bottles with screw caps to avoid kinetic fractionation through evaporation. All the samples were kept below 4 °C until they were analyzed. A Vantage Pro2 field weather station (Davis Instruments Corp., USA) was placed in the catchment area to monitor rainfall with a precision of 0.2 mm.

Major cations (K^+, Na^+, Ca^{2+}, and Mg^{2+}) were measured by inductively coupled plasma optical emission spectrometry (Perkin Elmer Optima 2100 ICP-OES, USA) with a precision of 0.01 mg/L. Major anions (Cl^-, NO_3^-, and SO_4^{2-}) were measured by ion chromatography (IC) with a resolution of 0.01 mg/L. The results indicate an estimated analytical error of >5%.

For the $\delta^{13}C_{DIC}$ analysis, a 10-μL water sample was injected into glass bottles that were pre-filled with 1 ml of the 85% phosphoric acid and had a magnetic stir bar. The CO_2 was extracted and purified following the cryogenic removal of H_2O using a liquid nitrogen-ethanol trap. The carbon isotope of the CO_2 was measured using a Gas Bench-linked with a Delta V Plus gas stable isotope-ratio mass spectrometer (Gasbench-IRMS).The results were calibrated using the international standard Vienna Pee Dee Belemnite (V-PDB) according to the following formula:

$$\delta^{13}C(‰) = \left[\left(R_{sample}/R_{standard}\right) - 1\right] \times 1000, \quad (1)$$

where $R = (^{12}C/^{13}C)$, R_{sample} is the relative abundance of the sample, $R_{standard}$ is the relative abundance of the standard, and the analytical error is less than 0.15%.

The oxygen and hydrogen isotopes ($\delta^{18}O$ and δD) of the water were measured by a liquid water stable isotope analyzer (LWIA-24d, Los Gatos Research, USA), which used the off-axis integrated cavity output spectroscopy technique (OA2ICOS). The isotope compositions were reported in standard δ-notation to represent the values in terms of per mil deviations from the V-SMOW standard (Vienna Standard Mean Ocean Water), the formulas of which are as follows:

$$\delta D‰ = \left[\left(\delta D/\delta H_{sample} - \delta D/\delta H\right)/\delta D/\delta H_{standard}\right] \times 1000, \quad (2)$$

$$\delta^{18}O‰ = \left[\left(\delta^{18}O/\delta^{16}O_{sample} - \delta^{18}O/\delta O_{standard}\right)/\delta^{18}O/\delta^{16}O_{standard}\right] \times 1000. \quad (3)$$

The precisions for δD and $\delta^{18}O$ are ±0.6 and ±0.2%, respectively. 50% of the samples were randomly selected for parallel analysis, and the results were within the error range. The cations, anions, $\delta^{13}C_{DIC}$, $\delta^{18}O$, and δD were all measured at the Institute of Karst Geology, Chinese Academy of Geological Sciences.

The saturation index of calcite (SIc) and the partial pressure of carbon dioxide (PCO_2) of the water were calculated from the hydrochemical data, which include the water temperature, pH, and concentrations of the seven major ions (K^+, Na^+, Ca^{2+}, Mg^{2+}, Cl^-, SO_4^{2-}, and HCO_3^-), using the modified WATSPEC program (Wigley 1977). The equation for the calculations of PCO_2 is presented as follows:

$$PCO_2 = \left(HCO_3^-\right) \times (H^+)/K_h \times K_1, \quad (4)$$

where K_h and K_1 are the temperature-dependent Henry's Law constants for CO_2 and the dissociation constant for H_2CO_3 in water, respectively. The equation used to calculate SIc is presented as follows:

$$SIc = Log\left(Ca^{2+}\right) \times \left(CO_3^{2-}\right)/K_c, \quad (5)$$

where K_c is the calcite equilibrium constant. If $SIc > 0$, then supersaturation occurs and calcium carbonate may precipitate; if $SIc < 0$, water is undersaturated with respect to calcite; and if $SIc = 0$, water is in equilibrium with respect to calcite.

Results and discussion

Hydrogeochemical characteristics of the subterranean stream

As shown in Table 1, the water temperature of the GSS ranged from 20.0 to 21.4 °C with an average of 20.8 °C during the dry season, and from 19.4 to 21.7 °C with an average of 20.6 °C during the wet season. The water temperature of the GSS exhibited a small change throughout the year such that the temperature was a relatively stable value and was close to the local multi-annual average air temperature (20 °C), thereby indicating that the GSS is a shallow karst groundwater and possesses a stronger regulatory role in relation to the external temperature changes. In addition, the water temperature of the GSS did not present a significant correlation with the other physical and chemical parameters (Table 2), thereby indicating the water temperature minimally influences the hydrogeochemical changes of the GSS.

The specific conductivity (SpC) of the GSS ranged from 459 to 482 μs/cm with an average value of 471 μs/cm during the dry season, and from 308 to 478 μs/cm with an average value of 431 μs/cm in the wet season. The SpC of the GSS during the dry season was greater and more stable than that of the wet season, whereas the SpC of the

Table 1 Statistic values of the hydrogeochemistry of the sampling sites

	T (°C)	pH	SpC (μs/cm)	K^+ (mg/L)	Na^+ (mg/L)	Ca^{2+} (mg/L)	Mg^{2+} (mg/L)	HCO_3^- (mg/L)	Cl^- (mg/L)	NO_3^- (mg/L)	SO_4^{2-} (mg/L)
(Dry season) $n = 12$											
Min	20.0	7.1	459	0.2	0.3	63.7	8.1	262.3	1.9	7.9	8.7
Max	21.4	7.5	482	0.5	1.0	105.9	14.2	298.9	2.9	10.6	13.5
Mean	20.8	7.3	471	0.4	0.6	87.1	11.1	280.7	2.5	9.4	11.5
(Wet season) $n = 12$											
Min	19.4	7.3	308	0.2	0.2	57.5	5.93	170.8	1.3	0.3	2.9
Max	21.7	7.8	478	0.5	0.8	102.1	12.6	298.9	2.7	12.4	15.7
Mean	20.6	7.5	431	0.4	0.5	85.0	9.38	262.1	2.1	8.2	11.5

Table 2 Correlation matrix of the hydrogeochemical parameters of the sampling site

Season	Index	pH	SpC	T	K^+	Na^+	Ca^{2+}	Mg^{2+}	HCO_3^-	Cl^-	NO_3^-	SO_4^{2-}
Dry season	pH	1										
	SpC	−0.503	1									
	T	−0.168	0.138	1								
	K^+	−0.611[a]	−0.149	0.141	1							
	Na^+	−0.719[b]	−0.054	0.141	0.948[b]	1						
	Ca^{2+}	−0.501	0.560[a]	−0.360	−0.756[b]	−0.777[b]	1					
	Mg^{2+}	0.389	0.102	−0.263	−0.276	−0.494	0.461	1				
	HCO_3^-	−0.043	0.595[a]	−0.135	−0.675[a]	−0.547[a]	0.561[a]	0.220	1			
	Cl^-	0.393	−0.150	−0.385	0.045	−0.137	−0.019	0.726[b]	−0.264	1		
	NO_3^-	−0.565	0.262	0.458	0.695[a]	0.715[b]	−0.625[a]	−0.211	−0.327	0.005	1	
	SO_4^{2-}	−0.441	0.009	0.007	0.456	0.523[a]	−0.500	−0.086	−0.019	0.151	0.621[a]	1
Wet season	pH	1										
	SpC	−0.253	1									
	T	0.306	−0.367	1								
	K^+	−0.538[a]	0.215	−0.421	1							
	Na^+	−0.637[a]	0.295	−0.434	0.830[b]	1						
	Ca^{2+}	−0.216	0.781[b]	−0.203	−0.145	0.138	1					
	Mg^{2+}	−0.351	0.451	0.001	−0.113	0.180	0.624[a]	1				
	HCO_3^-	−0.218	0.970[b]	−0.331	0.168	0.269	0.804[b]	0.387	1			
	Cl^-	−0.154	0.416	−0.215	0.009	0.046	0.676[a]	0.615[a]	0.417	1		
	NO_3^-	−0.204	0.770[b]	−0.526	0.219	0.255	0.806[b]	0.417	0.789[b]	0.813[b]	1	
	SO_4^{2-}	−0.277	0.813[b]	−0.337	0.146	0.174	0.837[b]	0.274	0.866[b]	0.653[a]	0.904[b]	1

[a] Correlation is significant at the 0.05 level

[b] Correlation is significant at the 0.01 level

wet season exhibited a greater fluctuation. The SpC minimum value (308 μs/cm) occurred in May, thereby indicating the possibility that the GSS was influenced by the dilution effect of the storms. The SpC presented a good positive correlation with Ca^{2+} and HCO_3^- during the study period (Table 2), thereby indicating the effect of karstification on the SpC. The pH of the GSS ranged from 7.1 to 7.5 and had a mean of 7.3 during the dry season, and ranged from 7.3 to 7.8 with a mean of 7.5 during the wet season, which presented weak alkalinity and small fluctuations throughout the year.

The changes in the composition of the subterranean stream solute were mainly influenced by the material source, though it is often affected by natural conditions (such as lithology, soil, atmospheric sedimentation, etc.) and human activities (such as industry, agriculture, city, etc.). The Gibbs model diagram is a useful semi-logarithmic plot that clearly and simply exhibits displays the

sources of various ions in the natural water (Gibbs 1970). The middle part of the Gibbs diagram indicates the significant control of the water–rock interaction on the water chemistry characteristics, while the upper right corner is mainly controlled by evaporation and crystallization, and the lower right angle is mainly controlled by rainfall. The samples from the dry and wet seasons, which are presented in Fig. 2, almost overlap, thereby indicating the water–rock interaction effects on the GSS throughout the year and the weakness of the precipitated solute input.

The triangular diagrams of the anions and cations present the relative importance of the different water–rock interactions required to supply ions to the water. The variations in the chemical composition of the GSS water are presented in Fig. 3. The GSS water was dominated by Ca^{2+} and HCO_3^-, which accounted for more than 89% of the total cations and anions. Of the cations, Ca^{2+} was the most dominant and accounted for more than 84% in the dry season and 86% in the wet season, while Mg^{2+} was generally lower than 14% in the dry season and 13% in the wet season, and Na^+ and K^+ were the least abundant (under 2%). HCO_3^- anion was dominant with Cl^-, NO_3^-, and SO_4^{2-} and accounted for less than 10% of the anions throughout the year, thereby indicating that the GSS is a Ca-HCO_3 type, which is consistent with the developed stream in the carbonate of the Rongxian formation (D_3r, Upper Devonian) of the study area. This demonstrates the control of the carbonate erosion-precipitation process on the chemical characteristics of the subterranean stream.

In general, the dominant ions in the karst water, namely Ca^{2+}, Mg^{2+}, and HCO_3^-, are mainly derived from the karst matrix through dissolution or precipitation (White 1988). The Ca^{2+}, Mg^{2+}, and HCO_3^- ion contents of the GSS in the wet season were lower with a relatively large fluctuation given the influence of the rich rainfall. The minimum value occurred in the wet season and was the result of the dilution effect of rainfall and the strong dynamic changes in the groundwater (Guo et al. 2007). The Ca^{2+}, Mg^{2+}, and HCO_3^- ion contents of the GSS in the dry season were higher, whereas the wet season presented more relatively stable ion contents due to the longer residence time and stronger water–rock interactions in the aquifer. A good positive correlation was observed between the Ca^{2+} and HCO_3^- ions of the GSS (Table 2), thereby indicating the homogeneous nature of their source, i.e., both of them are derived from karstification. Accordingly, the karst equations are as follows:

$$CaCO_3 + CO_2 + HCO_3 = Ca^{2+} + 2HCO_3^-, \quad (6)$$

$$CaMg(CO_3)_2 + 2CO_2 + 2HCO_3 = Ca^{2+} + Mg^{2+} + 4HCO_3^-, \quad (7)$$

$$CaCO_3 + CaMg(CO_3)_2 + 3CO_2 + 3HCO_3 = 2Ca^{2+} + Mg^{2+} + 6HCO_3^-. \quad (8)$$

The ratio of $c(Mg^{2+})/c(Ca^{2+})$ in the water was controlled by the proportion of calcite and dolomite in the stratum (White 1988). The ratio of $c(Mg^{2+})/c(Ca^{2+})$

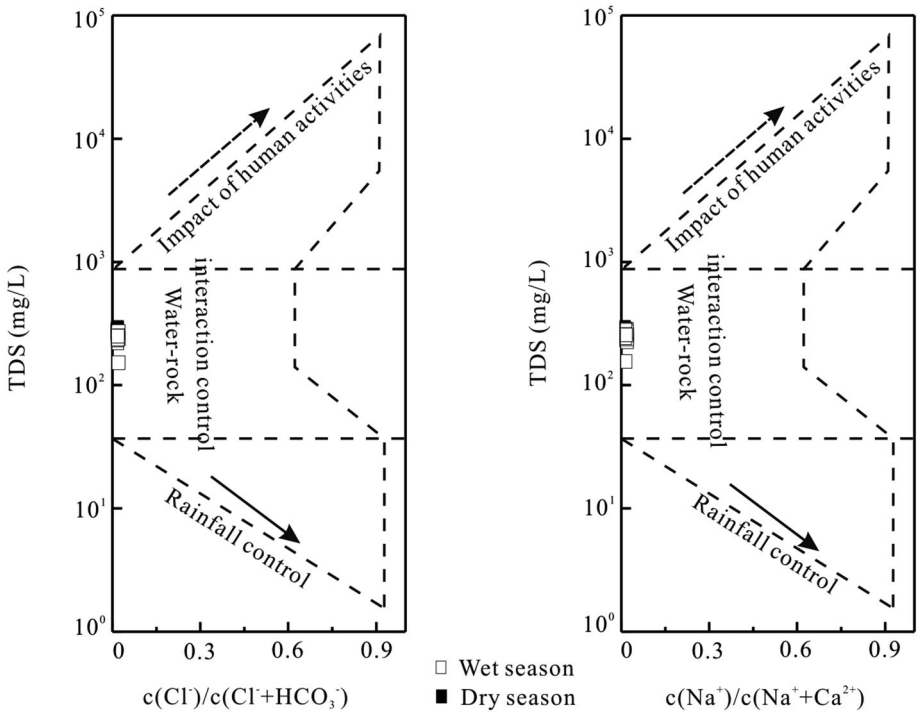

Fig. 2 Gibbs plot of the hydrogeochemistry of the sampling sites

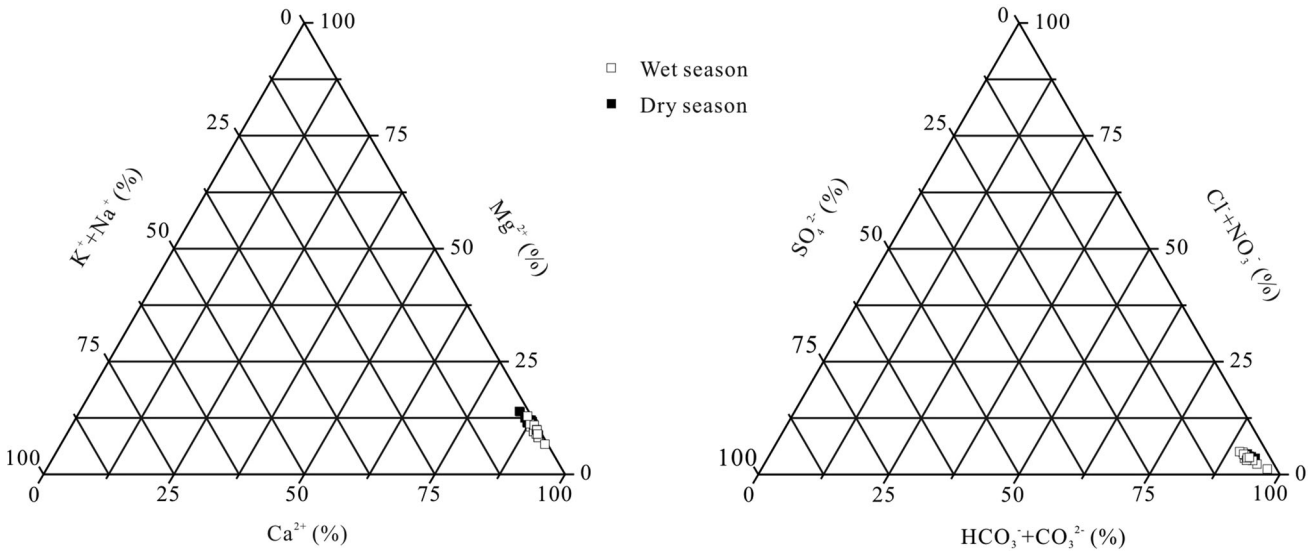

Fig. 3 Triangular diagrams of the anions and cations

indicates that carbonate rocks were the source of the solute (Pu et al. 2013). When the pure calcite dissolution was in equilibrium in the water, the $c(Mg^{2+})/c(Ca^{2+})$ was 0. When the pure dolomite dissolution was in equilibrium in the water, the $c(Mg^{2+})/c(Ca^{2+})$ is 1. When the calcite and dolomite dissolution are in equilibrium in the water, the $c(Mg^{2+})/c(Ca^{2+})$ is 0.5. Therefore, the calcite and dolomite contribution on the underground water chemistry can be determined based on the variation of the $c(Mg^{2+})/c(Ca^{2+})$ value. As shown in Fig. 4, the solute component of the subterranean stream was mainly derived from the dissolution of the calcite. In addition, according to the karst equation, the water–rock interactions produced Ca^{2+} and HCO_3^- ions in the GSS during both the dry and wet seasons, thereby indicating that the chemical characteristics of the groundwater were controlled by the calcite dissolution-precipitation process.

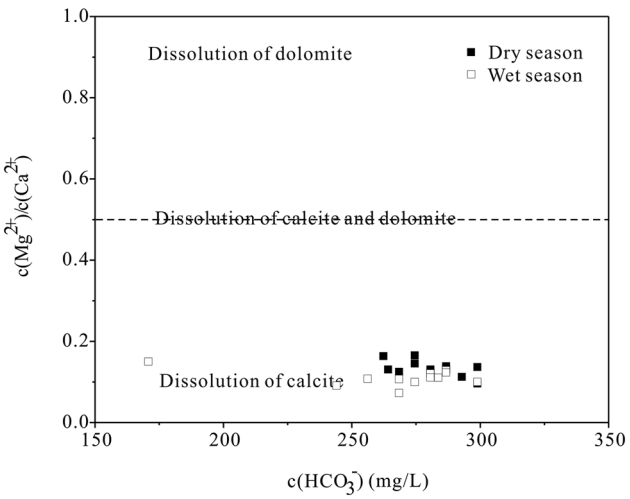

Fig. 4 Correlation between $c(Mg^{2+})/c(Ca^{2+})$ and $c(HCO_3^-)$

The concentration of NO_3^- in the GSS ranged from 7.9 to 10.6 mg/L with an average value of 9.4 mg/L in the dry season and from 0.3 to 12.4 mg/L with an average value of 8.5 mg/L in the wet season. The World Health Organization (WHO) noted that drinking water with a nitrate content exceeding l0 mg/L will have a significant impact on human health. The concentration of NO_3^- in the GSS was more than 10 mg/L during some months, thereby indicating that the GSS experienced a certain degree of nitrate pollution. The concentration of SO_4^{2-} in the GSS ranged from 8.7 to 13.5 mg/L with an average value of 11.6 mg/L in the dry season and from 2 to 15.6 mg/L with an average value of 11.5 mg/L in the wet season. NO_3^- and SO_4^{2-} exhibited a strong positive correlation in both the dry and wet seasons. In fact, the correlation coefficient was as high as 0.90 in the wet season (Table 2), thereby indicating that NO_3^- and SO_4^{2-} have the same source. The average concentrations of Cl^- and Na^+ in the GSS are 2.6 mg/L and 0.6 mg/L in the dry season, respectively, and 2.2 mg/L and 0.5 mg/L in the wet season, respectively. The Cl^-/Na^+ ratios of the samples were all greater than 1 (Fig. 5). This excess in Cl^- relative to Na^+ suggests additional Cl^- contributions from other sources (Ma et al. 2011). For example, the chemical fertilizers and manure were used in agricultural activities, and thousands of goats and ducks were fed in the fields (Guo and Jiang 2009), which may contribute to an increase in the concentration of Cl^-. In addition, NO_3^- and Cl^- as well as Cl^- and SO_4^{2-} exhibited good positive correlations during the wet season, thereby revealing that NO_3^-, Cl^-, and SO_4^{2-} may have been influenced by human activities in the wet season. However, the concentrations of Cl^-,

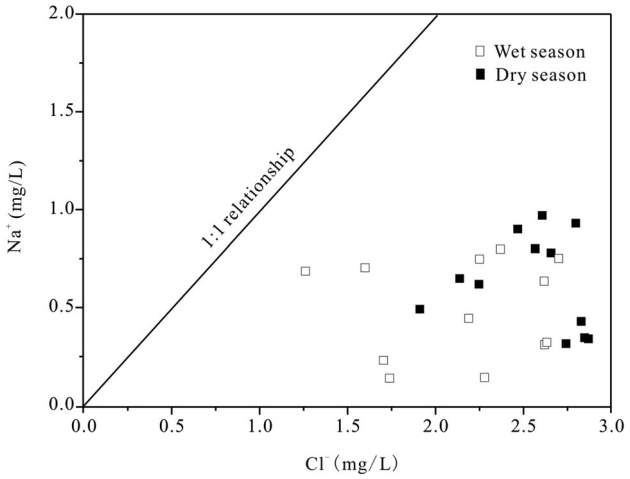

Fig. 5 Plot of Cl^- vs. Na^+ for the GSS

Na^+, NO_3^-, and SO_4^{2-} in the dry season were higher than those in the wet season, which was likely a result of agricultural activities that were performed during the wet season. The concentrations of Cl^-, Na^+, NO_3^-, and SO_4^{2-} in the wet season presented more fluctuations than those in the dry season, thereby indicating that the seasonal variations of Cl^-, Na^+, NO_3^-, and SO_4^{2-} in the GSS were affected by two factors: (1) human activity, mainly including agricultural activities and domestic sewage; (2) rainfall, which simultaneously generated increased groundwater pollutants and dilution effects (Yang 2010).

Although the chemical characteristics of the GSS were influenced by the water–rock interaction, human activities, and the dilution of rainfall during the monitoring period, the change in the CO_2 concentration in the water majorly affected the dissolution-precipitation of calcite as it controlled the variation of the underground water chemistry by affecting the pH and PCO_2 of the groundwater (Pu et al. 2013). The pH and PCO_2 exhibited a good negative correlation (Fig. 6), thereby indicating that their changes were controlled by a common factor, i.e., the CO_2 concentration of the GSS, which then caused karstification. High PCO_2 and low pH values in the water, indicate a strong corrosive ability, which results in a high HCO_3^- and Ca^{2+} in the water. In contrast, low PCO_2 and high pH values in the water indicate a weak corrosive ability, which results in a low HCO_3^- and Ca^{2+} in the water (Yuan 2002).

The calcite saturation index (SIc) ranged from −0.03 to 0.38 in the dry season and from 0.11 to 0.67 in the wet season. The dolomite saturation index (SId) ranged from −0.74 to −0.01 in the dry season and from −0.60 to −0.07 in the wet season. Almost all of the GSS water samples were oversaturated with respect to calcite and under-saturated with respect to dolomite (Fig. 7). The results agreed with the stream developed in the carbonate of the Rongxian formation (D_3r, Upper Devonian) in the study area. It is once again concluded that the chemical characteristics of the GSS are mainly controlled by the dissolution-precipitation process of calcite. In addition, the oversaturation of calcite indicates a prolonged water–rock interaction and indicates that carbonate dissolution is a major geochemical process that leads to such a saturation state.

Hydrogen and oxygen isotopic composition in the subterranean stream

In the dry season, the groundwater $\delta^{18}O$ and δD of the GSS ranged from −5.61 to −6.58% and −33.88 to −1.98%, respectively. The averages of the $\delta^{18}O$ and δD were −6.13% and −37.80%, respectively. In the wet season, the groundwater $\delta^{18}O$ and δD of the GSS ranged from −4.98 to −6.45% and −27.31 to −42.07%, respectively. The averages of the $\delta^{18}O$ and δD were −5.67 and −34.99% in

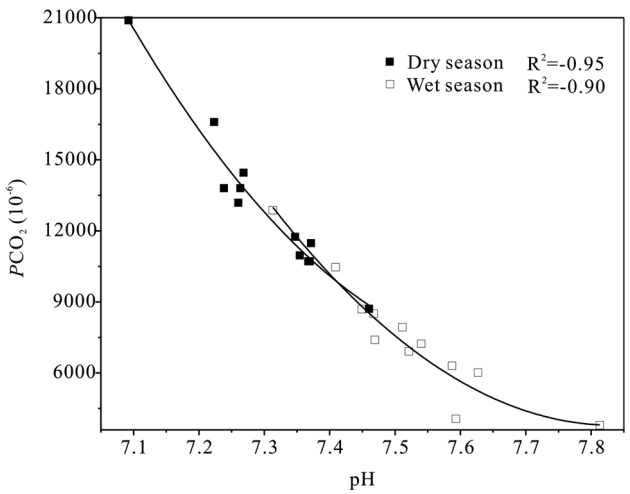

Fig. 6 Correlation between the pH value and PCO_2

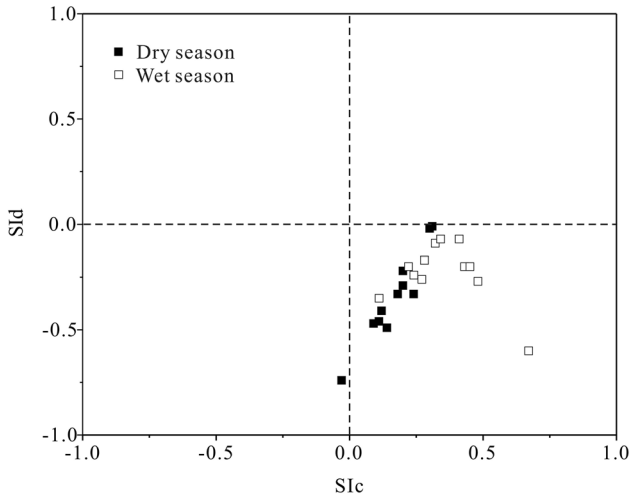

Fig. 7 Variation of SId vs. SIc

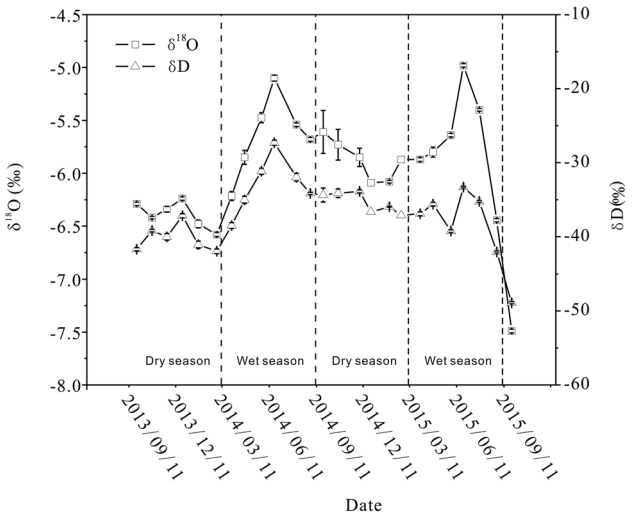

Fig. 8 Seasonal variation of the hydrogen and oxygen isotopes in the subterranean stream outlet

the wet season, respectively (Fig. 8). The variation trend between the $\delta^{18}O$ and δD of the GSS was identical during the 2-year monitoring period (Fig. 8). The global atmospheric precipitation isotope had an equation of $\delta D = 8\delta^{18}O + 10$ and the GMWL is the global meteoric water line, as presented in Fig. 9 (Craig 1961). The local meteoric water line (LMWL) had an equation of $\delta D = 8.42\delta^{18}O + 16.28$, which was established by 16-years' worth of oxygen and hydrogen isotopic data from Guilin precipitation (Tu et al. 2004), which is 105 km directly away from the GSS. The $\delta^{18}O$ and δD values of the GSS groundwater exhibited a significant positive correlation during the 2 years. The regression equations for $\delta^{18}O$ and δD are $\delta D = 7.48\delta^{18}O + 7.36$ ($R^2 = 0.63$, $P < 0.01$) during the wet season and $\delta D = 8.52\delta^{18}O + 14.47$ ($R^2 = 0.79$, $P < 0.01$) during the dry season. The $\delta^{18}O$ and δD values of the GSS in Fig. 9 fell around the GMWL and LMWL, thereby indicating that the source of the groundwater is rainwater. However, a relatively large disparity between the slope of the equation for the wet season and the slope of the LMWL was observed, and the $\delta^{18}O$ and δD values for the wet season deviated farther and were even shifted to the lower right of the global atmospheric water line. These results illustrate that the $\delta^{18}O$ and δD values, especially the values for the wet season, may be influenced by evaporation.

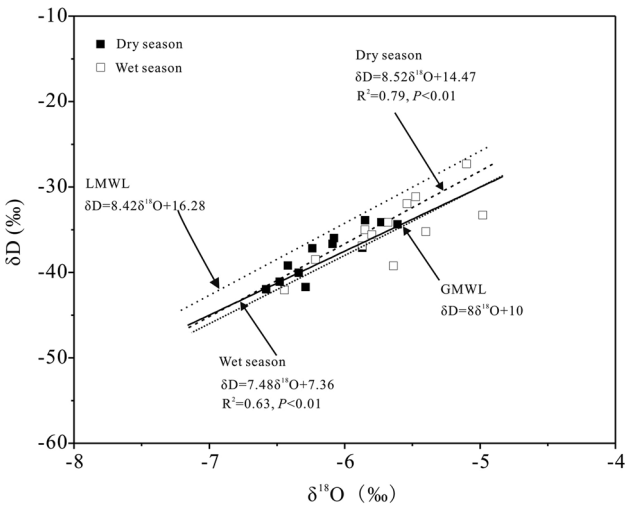

Fig. 9 Plot of $\delta^{18}O$ vs. δD for the waters in the subterranean stream outlet

The $\delta^{18}O$ and δD values for the wet season exhibited significant fluctuations as compared to the values of the dry season. There were no correlations among $\delta^{18}O$, δD, rainfall, and air temperature in the GSS during the wet season (Table 3), thereby indicating that the $\delta^{18}O$ and δD values of the GSS may have been affected by evaporation. Marfia et al. (2004) stated that the slope of the $\delta^{18}O$ and δD linear equation for the wet season was closer to the LMWL than the slope of the dry season, thereby indicating that precipitation during the wet season had a stronger ability to directly recharge groundwater as compared to the dry season. Some studies also found that most of the subterranean streams were directly and quickly recharged by precipitation (Marfia et al. 2004; Azzaz et al. 2008) from the karst conduits, fissures, sinkholes, and swallow holes present in the catchment area (Marfia et al. 2004). These studies indicate that the $\delta^{18}O$ and δD values for the wet season were not affected or were only lightly affected by evaporation in the karst areas. However, as shown in Fig. 1, the transformation of the GSS into a surface river and its relatively long flow time on the surface during the wet season may have affected the GSS water with regard to a certain degree of evaporation during the recharging groundwater by precipitation and surface water in the wet season. Meanwhile, the major agricultural activities were concentrated in the depression areas, which were frequently flooded during the wet season, and the tillage stage that occurred during the wet season. As a result, a large amount of irrigation water entered the groundwater system, thereby enhancing the effect of evaporation during the wet season (Chen et al. 2006).

Dansgaard (1964) proposed the concept of deuterium excess (*d*-excess) (defined as $d = \delta D - 8\delta^{18}O$), in which the *d* value is 10% for the Craig global meteoric water line as a way to compare the difference between the regional meteoric water line and the global meteoric water line. Different *d* values were calculated for various regions to represent the degree of isotopic fractionation during the evaporation and condensation processes of regional and atmospheric precipitation compared to global atmospheric precipitation (Dansgaard 1964; Wang 1991; Marfia et al. 2004). The *d* values for the GSS ranged from 8.62 to

Table 3 Correlation between $\delta^{18}O$, δD, air temperature, and rainfall for the dry and wet seasons

	$\delta^{18}O$	δD
Wet season		
Air temperature	$R^2 = 0.17$, $P = 0.180$	$R^2 = 0.04$, $P = 0.538$
Rainfall	$R^2 = 0.19$, $P = 0.085$	$R^2 = 0.08$, $P = 0.366$
Dry season		
Air temperature	$R^2 = 0.13$, $P = 0.259$	$R^2 = 0.02$, $P = 0.637$
Rainfall	$R^2 = 0.06$, $P = 0.227$	$R^2 = 0.03$, $P = 0.575$

12.92% in the dry season and from 5.87 to 13.49% in the wet season, with an average *d* value of 11.21% for the dry season and 10.5% for the wet season. The calculated *d* values for the atmospheric precipitation were within the range of 15–20% in the dry season and 2.5–12% in the wet season, and the average *d* values for atmospheric precipitation were 16.65% in the dry season and 10.50% in the wet season (Tu et al. 2004). The seasonal variation of the *d* values in the GSS were small compared to that of the *d* values for the atmospheric precipitation, which may be related to the different recharge events, the migration process of the subterranean stream, and the mixing of the different water sources. Some studies reported the groundwater *d* values between the average *d* values of precipitation in the dry and wet seasons, thereby indicating that the groundwater inherited the basic characteristics of precipitation (Deshpande et al. 2003). However, the *d* values of the GSS during the partial time periods, especially during the 2015 wet season, were lower than the *d* value of precipitation in the wet season. Moreover, an identical variation trend was observed between $\delta^{18}O$ and δD of the GSS, thereby indicating that the $\delta^{18}O$ and δD values were both enriched and affected by evaporation in the wet season.

Isotopic geochemical characteristics of $\delta^{13}C_{DIC}$ in the subterranean stream

The present study used the concentration of HCO_3^- as an approximation of the DIC concentration given that the HCO_3^- constituted for >90% of the DIC over a pH range of 7.3–8.5 (Rice et al. 2012), and the pH range in the GSS was 7.1–7.8 (Table 1). The DIC concentration of the GSS ranged from 262.3 to 298.9 mg/L in the dry season and from 170.8 to 298.9 mg/L in the wet season. The average value was 280.6 mg/L in the dry season and 262.3 mg/L in the wet season. The average DIC concentration in the wet season was lower than that in the dry season (Table 1), which may have been a result of the rainfall dilution. In the dry season, the $\delta^{13}C$ value of the GSS ranged from −13.5 to −11.3% with an average value of −12.4%. In the wet season, the $\delta^{13}C$ value of the GSS ranged from −13.9 to −9.5% with an average of −12.1%. The $\delta^{13}C$ values of the

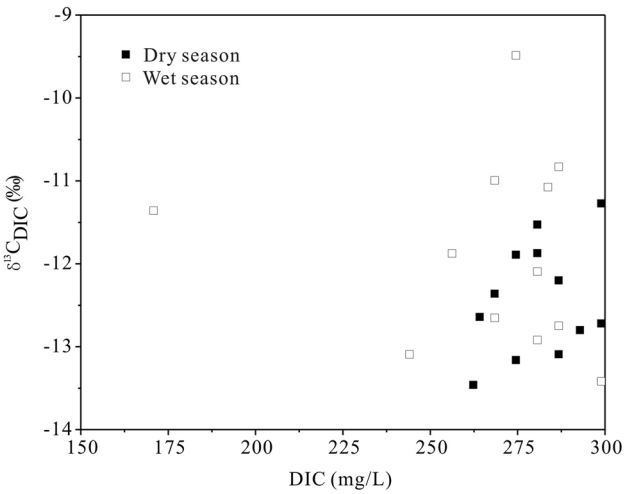

Fig. 10 Seasonal changes in DIC and $\delta^{13}C_{DIC}$ for the GSS

GSS in the wet season exhibited significant more fluctuations as compared to the dry season (Fig. 10), thereby indicating that the sources of carbon in the GSS was more complex during the wet season. In addition, the DIC and $\delta^{13}C$ of the GSS did not show any correlations ($r = -0.08$), thereby indicating the $\delta^{13}C$ values of the GSS was affected by multiple carbon sources. These conclusions were consistent with the findings on the relationship between the DIC and $\delta^{13}C$ of the GSS of a karst area, which was located in Guiyang (Li et al. 2005), the Shuicheng Basin (Li et al. 2010), and the Raisin river area of the exposed Paleozoic carbonate rocks in the entire Canadian basin (Cane and Clark 1999).

The DIC of the karst groundwater was mainly derived from atmospheric CO_2, soil CO_2 produced by the degradation of organic matter and plant root respiration, and the dissolution of carbonate minerals (Telmer and Veizer 1999). In addition, the study area is a typical acid rain affected area in China (Tang et al. 2010), has low precipitation and pH values, and contains a high concentration of sulfate, which promotes the dissolution of carbonate rock and increases the DIC (Pu 2011). Given the large variation of the $\delta^{13}C$ values in the different carbon sources, $\delta^{13}C$ can be used to trace the sources and the transformation of carbon in groundwater (Clark and Fritz 1997).

The study area is in the southwest acid rain area of the Chongqing-Guiyang-Liuzhou area of China and has a mean annual pH of 4.5–5 (Tang et al. 2010). The presented range has a very low DIC content in rainwater, specifically about $1 \times 10^{-2} - 5 \times 10^{-2}$ mmol/L (Stumm and Morgan 1996). Therefore, the contribution of rainwater to the DIC of the groundwater can be assumed negligible. In recent years, due to the emissions of fossil fuels, the content of CO_2 in the atmosphere has increased from 280×10^{-6} before the industrial revolution to 400.72×10^{-6} at present (http://www.esrl.noaa.gov/gmd/ccgg/trends/global.html), while its $\delta^{13}C$ value decreased from −6.4 to −7.6% (Friedli et al. 1986; Zhang et al. 1995). Because the amount of CO_2 in the underground water is much larger than that in the atmosphere, the amount of diffusion from the air to the groundwater is very low, e.g., the minimum PCO_2 value of the GSS in the study area was 4073.80×10^{-6} during the monitoring period. Therefore, the present study ignored the influence of the $\delta^{13}C$ of the atmospheric CO_2 on the $\delta^{13}C$ of the DIC in the groundwater. Likewise, the DIC sources in the groundwater were scaled to two end-members, including the soil CO_2 and the DIC produced by carbonate mineral dissolution.

The soil CO_2 mainly originated from the respiration of plants and the degradation of organic matter. Soil CO_2 from C_3 plant respiration and organic matter degradation exhibited a $\delta^{13}C_{CO2}$ value that ranged from −30 to −24% with an average value of −27%, whereas the $\delta^{13}C_{CO2}$ value of C_4 plants ranged from −16 to −10% with an average value of −12.5% (Vogel 1993; Clark and Fritz 1997). CO_2 produced by the oxidation of organic matter in the soil hardly generated fractionation (Palmer et al. 2001), though CO_2 diffusion in soil produced 4% fractionation (Cerling et al. 1991). Therefore, an estimated average $\delta^{13}C_{CO2}$ value of −23% for C_3 vegetation and −9% for C_4 vegetation was observed. Because C_3 vegetation was mainly distributed in the study area, the soil $\delta^{13}C_{CO2}$ value was influenced by the CO_2 of the C_3 vegetation in the study area, which was about −23% in theory. Soil CO_2 was dissolved by rainwater and was subsequently converted to DIC, thereby resulting in an average fractionation of 9% (Zhang et al. 1995). Therefore, the groundwater exhibited a $\delta^{13}C_{DIC}$ value of about −14% under C_3 vegetation. Carbonate is generally a marine deposit; thus, the $\delta^{13}C_{carbonate}$ value was about $0 \pm 1\%$. The present study assigned the 0% average as the $\delta^{13}C_{carbonate}$ initial value. In an open system, the DIC in groundwater constantly receives a supply of CO_2 from the external environment, thereby generating a final $\delta^{13}C_{DIC}$ of about −14% for C_3 vegetation, which is composed of soil and atmospheric CO_2 (Deines et al. 1974; Clark and Fritz 1997). In a closed system, the soil CO_2 supply was continuously reduced such that the $\delta^{13}C_{DIC}$ value of the groundwater was about −11.5% for C_3 vegetation, which was controlled by the dissolution equilibrium between the soil and the carbonate minerals (Fig. 11). Therefore, the theoretical $\delta^{13}C_{DIC}$ value of the groundwater was theoretically calculated to be around −14% or −11.5%.

The $\delta^{13}C_{DIC}$ values of the GSS water in Fig. 11 do not correspond to the expected $\delta^{13}C_{DIC}$ value derived from either an open or closed system. The GSS values may have been a result of the fluctuation in the groundwater level and the change in the hydrodynamic conditions, thereby resulting in the conversion of the carbonate rock evolution between the closed and open system (Jiang et al. 2013). Therefore, the GSS was determined to be a semi-open system with an $\delta^{13}C_{DIC}$ value in the GSS created by the $\delta^{13}C_{DIC}$ value of different sources at different proportions, which results in a significant difference between the calculated $\delta^{13}C_{DIC}$ value of the karst groundwater and the theoretical value. According to the mass balance principle, the $\delta^{13}C_{DIC}$ value of groundwater can be calculated as follows (Chapelle and Knobel 1985; Fang et al. 2000; Li et al. 2005):

$$\delta^{13}C_{DIC} = \left[\sum_{0}^{i}(mCi)(\delta^{13}Ci)\right] / \left[\sum_{0}^{i}(mCi)\right], \quad (9)$$

where $\delta^{13}C_{DIC}$ is the measured value for the groundwater, mCi is the DIC content from the ith source, and $\delta^{13}Ci$ is the $\delta^{13}C$ composition of the DIC from the ith source. The $\delta^{13}C_{DIC}$ value of the subterranean stream is controlled by two end-members, including the soil CO_2 and the dissolution of the carbonate rocks, based on Eq. 9. The formula can be simplified as follows:

$$\delta^{13}C = \delta^{13}C_{carbonate} \times R_{carbonate} + \delta^{13}C_{soil} \times R_{soil} \quad (10)$$

$$R_{carbonate} + R_{soil} = 1, \quad (11)$$

where $\delta^{13}C_{DIC}$ is the measured value of the groundwater, $\delta^{13}C_{carbonate}$ is the theoretical $\delta^{13}C$ value of carbonate, $\delta^{13}C_{soil}$ is the theoretical $\delta^{13}C$ value of soil CO_2, $R_{carbonate}$ is the proportion of the DIC derived from the carbonate to the total DIC of the stream, and R_{soil} is the proportion of DIC derived from the soil CO_2 to the total DIC of the stream. The contribution of the carbonate dissolution to the DIC in the GSS was calculated to be 50.2–58.3% with an average of 54.0% in the dry season, and 48.7–64.7% with an average of 55.2% for the wet season. The calculated values for the wet season exhibited a greater fluctuation as compared to those of the dry season, thereby suggesting that frequent storm events may have impacted the groundwater recharge conditions and carried a large amount of CO_2 in the soil into the groundwater system during the wet season (Pu 2011). In addition, according to the karstification equation

$$Ca_{1-x}Mg_xCO_3 + H_2CO_3 \rightarrow (1-x)Ca^{2+} + xMg^{2+} + 2HCO_3^-. \quad (12)$$

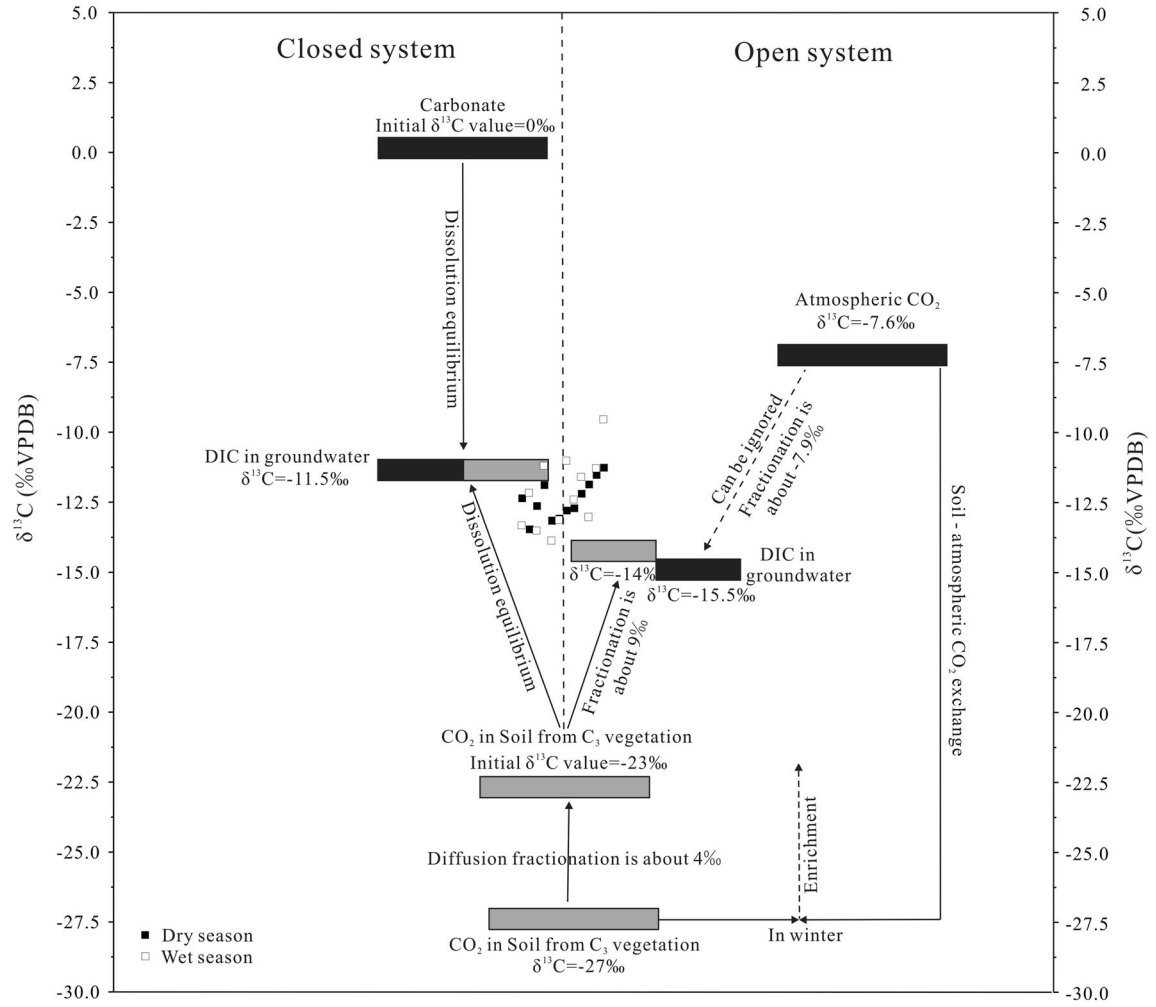

Fig. 11 Conceptual model of the DIC sources and the $\delta^{13}C$ evolution in an underground river

The contribution of carbonate dissolution to the DIC in the groundwater is assumed to be 50%, though the contributions in the GSS were almost all greater than 50% for both seasons, thereby indicating the presence of other inorganic acids such as sulfuric acid, which was formed from the oxidation of sulfides and nitric acid due to the participation of nitrification during carbonate dissolution. Therefore, in calculating the carbon sink of karstification, the proportion of carbonate dissolution contributing to the DIC of the groundwater must first be calculated.

Effects of human activities on the hydrogeochemical characteristics of groundwater

As described above, the chemical characteristics of the subterranean stream were influenced by the water–rock interaction. Ca^{2+} and HCO_3^- were the dominant ions in the GSS and the pollutants introduced by human activities,

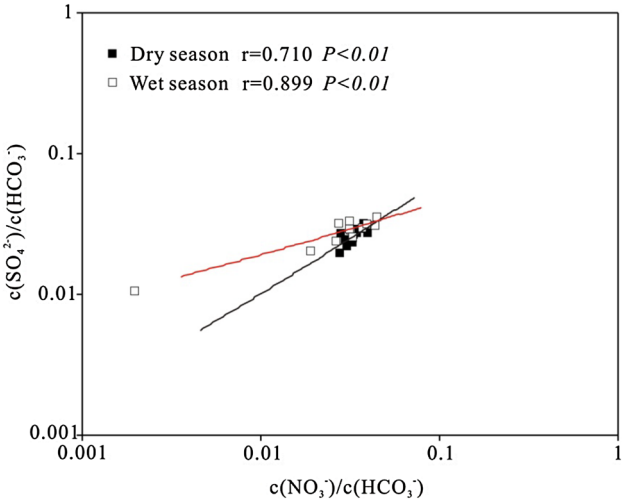

Fig. 12 Correlations of HCO_3^-, normalized NO_3^-, and SO_4^{2-} values (molar ratios) in the Guancun subterranean stream

including K^+, Na^+, Cl^-, NO_3^-, and SO_4^{2-}, were significantly smaller than the changes in carbonate dissolution (Fig. 3). However, the GSS experienced a certain degree of pollution for a few months, particularly with NO_3^- and SO_4^{2-} ions. Figure 12 presents the changing relationship between the NO_3^- and SO_4^{2-} ions. The $c(SO_4^{2-})/c(HCO_3^-)$ and $c(NO_3^-)/c(HCO_3^-)$ exhibit a strong correlation during both seasons, thereby indicating a constant supply of NO_3^- and SO_4^{2-} ions. Some studies have demonstrated that the notable increase in the nitrate and sulfate concentrations is a result of the utilization of a large amount of chemical fertilizers in agriculture (Aravena et al. 1999; Jiang et al. 2008). Guo et al. (2007) stated that the nitrate and sulfate exhibited an obvious increase within the past two decades in the GSS catchment area, thereby illustrating that the main source of NO_3^- and SO_4^{2-} ions was agricultural activities.

In recent years, many studies have indicated the presence of an additional proton-promoted weathering pathway of carbonate rocks in the agricultural areas due to an increase in NO_3^- and SO_4^{2-} ions, which affect the riverine alkalinity (Semhi et al. 2000; Spence and Telmer 2005; Perrin et al. 2008; Ali and Atekwana 2011; Gandois et al. 2011). The formulas for the dissolution of the carbonate rocks by nitric acid and sulfuric acid are

$$(Ca_{1-x}Mg_x)CO_3 + HNO_3 \rightarrow (1-x)Ca^{2+} + xMg^{2+} + HCO_3^- + NO_3^- \quad (13)$$

$$2(Ca_{1-x}Mg_x)CO_3 + H_2SO_4 \rightarrow 2(1-x)Ca^{2+} + 2xMg^{2+} + 2HCO_3^- + SO_4^{2-}. \quad (14)$$

The molar ratio between $(Ca^{2+} + Mg^{2+})$ and HCO_3^- is 1 for the nitric acid and sulfuric acid process, which affects the dissolution of carbonate. However, the karstification equation in Eq. 13 exhibits a molar ratio of 0.5 between $(Ca^{2+} + Mg^{2+})$ and HCO_3^- as carbonic acid dissolves carbonate. In Fig. 13, the molar ratio between $(Ca^{2+} + Mg^{2+})$ and HCO_3^- of most of the water samples in the GSS falls between 0.5 and 1 during the monitoring period. The molar ratio between $(Ca^{2+} + Mg^{2+})$ and HCO_3^- for the GSS ranged from 0.53 to 0.70 with an average value of 0.59 in the dry season and from 0.52 to 0.65 with an average value of 0.58 in the wet season (Fig. 13), which further demonstrates that the dissolution of the carbonate rock was affected not only by carbonic acid, but also by sulfuric acid and nitric acid.

The contribution proportion of the different acids for the dissolution of the carbonate rock can be calculated as follows:

$$f1 = 2\left[n\left(HCO_3^-\right) - n\left(Ca^{2+} + Mg^{2+}\right)\right]/n\left(HCO_3^-\right) \times 100\% \quad (15)$$

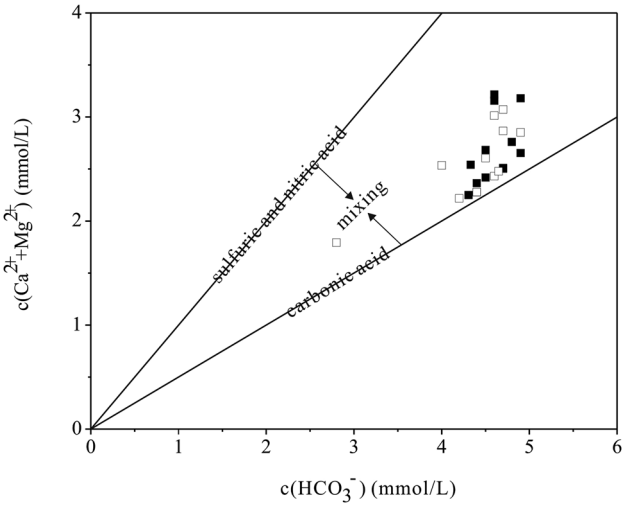

Fig. 13 Ratio between $Ca^{2+} + Mg^{2+}$ and HCO_3^- in the Guancun subterranean stream

$$f2 = \left[2n\left(Ca^{2+} + Mg^{2+}\right) - n\left(HCO_3^-\right)\right]/n\left(HCO_3^-\right) \times 100\% \quad (16)$$

$$f1 + f2 = 1 \quad (17)$$

where n represents the molar number of the substances, $f1$ represents the contribution rate of carbonic acid, and $f2$ represents the contribution rate of nitric acid and sulfuric acid. After this calculation, the contributions of carbonate dissolution due to carbonic acid to the total HCO_3^- concentration in the groundwater varied from 69.0 to 96.5% with a mean percentage of 83.6% in the wet season and from 60.1 to 94.9% with a mean percentage of 82.5% in the dry season. The contributions of the carbonate dissolution due to sulfuric acid and nitric acid to the total HCO_3^- concentration in the groundwater varied from 3.5 to 31% with a mean percentage of 16.4% in the wet season and from 5.1 to 39.9% with a mean percentage of 16.4% in the dry season.

According to Eqs. 13 and 14, the control of sulfuric acid and nitric acid on dissolution eliminates its consumption of atmospheric and soil CO_2, thereby releasing CO_2. Therefore, the presence of sulfuric acid and nitric acid can result in the loss of DIC (ΔHCO_3^-) during the dissolution of carbonate rock. The ΔHCO_3^- can be calculated from the difference between the theoretical ($HCO_3^-{}_{theoretical}$) and the measured DIC ($HCO_3^-{}_{measured}$) as follows:

$$\Delta HCO_3^- = HCO_{3_{theoretical}}^- - HCO_{3_{measured}}^- \quad (18)$$

$HCO_3^-{}_{theoretical}$ is deduced from the measured $Ca^{2+} + Mg^{2+}$ concentrations (mmol/L) using the theoretical molar ratio $(Ca^{2+} + Mg^{2+})/HCO_3^- = 0.5$ based on the natural carbonate dissolution by carbonic acid (Eq. 9). Following this calculation, due to the influence of sulfuric acid and nitric acid, a loss of DIC was calculated within the

range of 0.22–1.83 mmol/L with an average of 0.81 mmol/L in the dry season and within the range of 0.15–1.44 mmol/L with an average of 0.71 mmol/L in the wet season. These DIC losses indicate that half of the carbon sink may have been produced by carbonic acid given that atmospheric/soil CO_2 was not consumed during the dissolution of carbonate by sulfuric acid and nitric acid and in accordance with Eq. 12.

Conclusions

The chemical compositions of the GSS water in both the winter and summer were dominated by Ca^{2+} and HCO_3^-, which accounted for more than 89% of the total cations and anions. K^+, Na^+, Cl^-, NO_3^-, and SO_4^{2-} ions were affected by the residual component of agricultural fertilization, as evinced by their correlations. The hydrogeochemical processes of the GSS water were controlled by the water–rock interaction (i.e., calcite dissolution-precipitation processes) with a clear classification of the pure calcite, which exhibited a low Mg^{2+}/Ca^{2+} ratio. The pH and PCO_2 were controlled by the CO_2 concentration, which then drove the changes in the hydrogeochemical processes in the GSS water. The GSS reached oversaturation after a long period of water–rock–gas interaction, thereby concluding carbonate dissolution to be the major geochemical process given that almost all the GSS samples were oversaturated with respect to calcite.

The GSS water was concluded to be primarily sourced from precipitation given that the $\delta^{18}O$ and δD values of the GSS fell around the GMWL and LMWL. However, the GSS water may have been affected by evaporation due to the large amount of irrigation water entering the groundwater system and the transformation of the GSS into a surface river and its subsequent long flow time on the surface during the wet season. These permeations resulted in the deviation and shift of several $\delta^{18}O$ and δD values to the lower right of the global atmospheric water line.

The $\delta^{13}C_{DIC}$ values of the GSS water may have been affected by multiple carbon sources and did not correspond to the expected $\delta^{13}C_{DIC}$ value, thereby suggesting the presence of an open system–closed system carbonate evolution in the GSS water samples. Therefore, the $\delta^{13}C_{DIC}$ values of the GSS were formed by the $\delta^{13}C_{DIC}$ values of different sources at different proportions. The DIC sources in the GSS water were mainly composed of soil CO_2 and carbonate dissolution. According to the simplified mass balance formula, the contributions of the carbonate dissolution to the DIC of the GSS were 50.2–58.3% and 48.7–64.7% in the dry and wet seasons, respectively, thereby indicating that the contribution of carbonate dissolution in the formation of DIC in the karst groundwater was not necessarily 50%, which was the value calculated by the karstification formula. Nitric acid and sulfuric acid affected the dissolution of carbonate as it did not consume the atmospheric/soil CO_2 during the dissolution of carbonate. The calculations indicate that the presence of sulfuric acid and nitric acid resulted in the loss of DIC (ΔHCO_3^-) during the dissolution of the carbonate rock, and the amounts ranged from 0.22–1.83 mmol/L with an average of 0.81 mmol/L in the dry season and ranged from 0.15–1.44 mmol/L with an average of 0.71 mmol/L in the wet season. These DIC losses indicate that half of the carbon sink may have been produced by carbonic acid.

Acknowledgements The authors thank the support of the National Natural Science Foundation of China (No. 41572234 and No. 41402324), the Special Fund for Basic Scientific Research of the Chinese Academy of Geological Sciences (No. YYWF201636), the Key Research and Development Fund of Ministry of Science and Technology of China (No. 2016YFC0502501), the Special Fund for Public Benefit Scientific Research of the Ministry of Land and Resources of China (No. 201311148) and the Geological Survey Project of CGS (No. DD20160305-03). The authors also thank Wen Liu and Xue Mo for their assistance in the field.

Compliance with ethical standards

Conflict of interest The authors declare no conflicts of interest.

References

Al-Charideh A (2011) Environmental isotope study of groundwater discharge from the large karst springs in West Syria: a case study of Figeh and Al-sin springs. Environ Earth Sci 63(1):1–10

Ali HN, Atekwana EA (2011) The effect of sulfuric acid neutralization on carbonate and stable carbon isotope evolution of shallow groundwater. Chem Geol 284(3):217–228

Aravena R, Auge M, Bucich N (1999) Evaluation of the origin of groundwater nitrate in the city La Plata—Argentina, using isotope techniques. In: Drew D (ed) Hydrogeology and land use management. Congress of International Association of Hydrogeologists. Bratislava, pp 323–327

Azzaz H, Cherchali M, Meddi M, Houha B, Puig JM, Ahcachi A (2008) The use of environmental isotopic and hydrochemical tracers to characterize the functioning of karst systems in the Tlemcen Mountains, northwest Algeria. Hydrogeol J 16(3):531–546

Cane G, Clark ID (1999) Tracing ground water recharge in an agricultural watershed with isotopes. Ground Water 37(1):133–139

Cao JH, Yuan DX, Zhang C, Jiang ZC (2004) Karst ecosystem constrained by geological conditions in southwest china. Earth and environment 32(1):1–8 **(in Chinese with English abstract)**

Cerling TE, Solomon DK, Quade JAY, Bowman JR (1991) On the isotopic composition of carbon in soil carbon dioxide. Geochim Cosmochim Acta 55(11):3403–3405

Chapelle FH, Knobel LRL (1985) Stable carbon isotopes of HCO_3^- in the Aquia Aquifer, Maryland: evidence for an isotopically heavy source of CO_2. Ground Water 23(5):592–599

Chen ZY, Nie ZL, Zhang GH, Li W, Shen GM (2006) Environmental isotopic study on the recharge and residence time of groundwater

in the Heihe River Basin, northwestern China. Hydrogeol J 14(8):1635–1651

Clark I, Fritz P (1997) Environmental isotopes in hydrogeology. Lewis Publishers, New York

Craig H (1961) Isotopic variations in meteoric waters. Science 133(3465):1702–1703

Dansgaard W (1964) Stable isotopes in precipitation. Tellus 16(4):436–468

Deines P, Langmuir D, Harmon RS (1974) Stable carbon isotope ratios and the existence of a gas phase in the evolution of carbonate waters. Geochim Cosmochim Acta 3:1147–1164

Deshpande RD, Bhattacharya SK, Jani RA, Gupta SK (2003) Distribution of oxygen and hydrogen isotopes in shallow groundwaters from Southern India: influence of a dual monsoon system. J Hydrol 271:226–239

Fang JS, Barcelona MJ, Krishnamurthy RV, Atekwana EA (2000) Stable carbon isotope biogeochemistry of a shallow sand aquifer contaminated with fuel hydrocarbons. Appl Geochem 15(2):157–169

Friedli H, Lotscher H, Oeschger H, Siegenthaler U, Stauffer B (1986) Ice core record of the $^{12}C/^{13}C$ ratio of atmospheric CO_2 in The past two centuries. Nature 324:237–238

Gandois L, Perrin AS, Probst A (2011) Impact of nitrogenous fertiliser-induced proton release on cultivated soils with contrasting carbonate contents: a column experiment. Geochim Cosmochim Acta 75(5):1185–1198

Gibbs RJ (1970) Mechanisms controlling world water chemistry. Science 170(3962):1088–1090

Gonfiantini R, Zuppi GM (2003) Carbon isotope exchange rate of DIC in karst groundwater. Chem Geol 197(1):319–336

Gong CM, Ning PB, Wang GX, Liang ZS (2009) A review of adaptable variations and evolution of photosynthetic carbon pathway in C3 and C4 plants. Chin J Plant Ecol 33(1):206–221 **(in Chinese with English abstract)**

Guo F, Jiang G (2009) Nitrogen budget of a typical subterranean river in peak cluster karst area. Environ Geol 58(8):1741–1748

Guo F, Jiang G, Yuan D (2007) Major ions in typical subterranean rivers and their anthropogenic impacts in southwest karst areas. China Environ Geol 53(3):533–541

Han G, Tang Y, Wu Q (2010) Hydrogeochemistry and dissolved inorganic carbon isotopic composition on karst groundwater in Maolan, southwest China. Environmental Earth Sciences 60(4):893–899

Hu K, Chen H, Nie Y, Wang K (2015) Seasonal recharge and mean residence times of soil and epikarst water in a small karst catchment of southwest China. Scientific Reports 5

Jiang Y, Zhang C, Yuan D, Zhang G, He R (2008) Impact of land use change on groundwater quality in a typical karst watershed of southwest China: a case study of the Xiaojiang watershed. Yunnan Province. Hydrogeol J 16(4):727–735

Jiang YJ, Hu YJ, Schirmer M (2013) Biogeochemical controls on daily cycling of hydrochemistry and $\delta^{13}C$ of dissolved inorganic carbon in a karst spring-fed pool. J Hydrol 478:157–168

Kanduč T, Szramek K, Ogrinc N, Walter LY (2007) Origin and cycling of riverine inorganic carbon in the Sava River watershed (Slovenia) inferred from major solutes and stable carbon isotopes. Biogeochemistry 86(2):137–154

Lang YC, Liu CQ, Zhao ZQ, Li SL, Han GL (2006) Geochemistry of surface and ground water in Guiyang, China: water/rock interaction and pollution in a karst hydrological system. Appl Geochem 21(6):887–903

Lee KS, Kim Y (2007) Determining the seasonality of groundwater recharge using water isotopes: a case study from the upper North Han River basin, Korea. Environ Geol 52(5):853–859

Li SL, Liu CQ, Tao FX, Lang YC, Han GL (2005) Carbon biogeochemistry of ground water, Guiyang. Southwest China. Ground Water 43(4):494–499

Li XD, Liu CQ, Harue M, Li SL, Liu XL (2010) The use of environmental isotopic (C, Sr, S) and hydrochemical tracers to characterize anthropogenic effects on karst groundwater quality: a case study of the Shuicheng Basin, SW China. Appl Geochem 25(12):1924–1936

Liu ZH, Yuan DX, He SY (1997) Stable carbon isotope geochemical and hydrochemical features in the system of carbonate-H_20-CO_2 and their implications—Evidence from several typical karst areas of China. Acta Geol Sincia 71(3):281–288 **(in Chinese with English abstract)**

Liu ZH, Li Q, Sun H, Wang JL (2007) Seasonal, diurnal and storm-scale hydrochemical variations of typical epikarst springs in subtropical karst areas of SW China: soil CO_2 and dilution effects. J Hydrol 337(1):207–223

Ma R, Wang YX, Sun ZY, Zheng CM, Ma T, Prommer H (2011) Geochemical evolution of groundwater in carbonate aquifers in Taiyuan, northern China. Appl Geochem 26(5):884–897

Marfia AM, Krishnamurthy RV, Atekwana EA, Panton WF (2004) Isotopic and geochemical evolution of ground and surface waters in a karst dominated geological setting: a case study from Belize, Central America. Appl Geochem 19(6):937–946

Palmer SM, Hope D, Billett MF, Dawson JJ, Bryant CL (2001) Sources of organic and inorganic carbon in a headwater stream: evidence from carbon isotope studies. Biogeochemistry 52(3):321–338

Perrin AS, Probst A, Probst JL (2008) Impact of nitrogenous fertilizers on carbonate dissolution in small agricultural catchments: implications for weathering CO_2 uptake at regional and global scales. Geochim Cosmochim Acta 72(13):3105–3123

Peyraube N, Lastennet R, Denis A (2012) Geochemical evolution of groundwater in the unsaturated zone of a karstic massif, using the PCO_2–SIc relationship. J Hydrol 430:13–24

Pu JB (2011) Research on the controlling factors of formation and distribution of subterranean karst streams and its hydrogeochemistry regionality, Chongqing. Southwest University, China

Pu JB, Yuan DX, Jiang YJ, Gou PF, Yin JJ (2013) Hydrogeochemistry and environmental meaning of Chongqing subterranean karst streams in China. Advances in Water Science 34:713–722 **(in Chinese with English abstract)**

Rao NS, Rao KVS, Rao PS, Rao CV, Arjunudu K, Reddy MP, Subrahmanyam A (2009) Geochemistry of carbonate precipitation from the groundwater in a coastal region. J Geol Soc India 73(5):651–656

Rice EW, Baird RB, Eaton AD, Clesceri LS (2012) Standard methods for the examination of water and wastewater, 22nd edn. American Public Health Association, the American Water Works Association and the Water Environment Federation, Washington D.C

Sebela S, Liu H (2014) Structural geological characteristics of karst caves and major stone forest, Yunnan, China. Acta Carsologica 43:115–127

Semhi K, Suchet PA, Clauer N, Probst JL (2000) Impact of nitrogen fertilizers on the natural weathering-erosion processes and fluvial transport in the Garonne basin. Appl Geochem 15(6):865–878

Spence J, Telmer K (2005) The role of sulfur in chemical weathering and atmospheric CO_2 fluxes: evidence from major ions, $\delta^{13}C_{DIC}$, and $\delta^{34}S_{SO4}$ in rivers of the Canadian Cordillera. Geochim Cosmochim Acta 69(23):5441–5458

Stumm W, Morgan J (1996) Aquatie chemistry, chemical equilibria and rates in natural waters, 2nd edn. Wiley, Toronto

Tang J, Xu XB, Ba J, Wang SF (2010) The change trend of precipitation acidity in China during 1992–2006. Chin Sci Bull 55(8):705–712 **(in Chinese with English abstract)**

Taniguchi M, Nakayama T, Tase N, Shimada J (2000) Stable isotope studies of precipitation and river water in the Lake Biwa basin, Japan. Hydrol Process 14(3):539–556

Telmer K, Veizer J (1999) Carbon fluxes, PCO_2 and substrate weathering in a large northern river basin, Canada: carbon isotope perspectives. Chem Geol 159(1):61–86

Tillman FD, Oki DS, Johnson AG, Barber LB, Beisner KR (2014) Investigation of geochemical indicators to evaluate the connection between inland and coastal groundwater systems near Kaloko-Honokōhau National Historical Park, Hawai'i. App Geochem 51:278–292

Tu LL, Wang H, Feng YM (2004) Research on D and ^{18}O isotope in the precipitation of Guilin. Carsologica Sincia 23(4):305–309 **(in Chinese with English abstract)**

Verbovšek T, Kanduč T (2016) Isotope geochemistry of groundwater from fractured dolomite aquifers in Central Slovenia. Aquat Geochem 22(2):131–151

Vogel JC (1993) Stable isotopes and plant carbon-water relations. Academic Press, San Diego

Wang HC (1991) Isotope Hydrogeology. Geological Publishing House, Beijing

White WB (1988) Geomorphology and hydrology of karst terrains. Oxford University Press, New York

Wigley TML (1977) WATSPEC: a computer program for determining the equilibrium speciation of aqueous solutions. Geo-Abstracts for the British Geomorphological Research Group, pp 1–49

Yang PH (2010) The hydrogeochemical characteristics and transportation of suspended particle matters in Qingmuguan underground river system, Chongqing. Southwest University, China

Yuan DX (2000) Aspects on the new round land and resources survey in karst rock desertification areas of south China. Carsologica Sincia 19(2):103–108 **(in Chinese with English abstract)**

Yuan DX (2002) Karst dynamic system of China. Geology Press, Beijing **(In Chinese)**

Yuan J, Xu F, Deng G, Tang YQ (2017) Using stable isotopes and major ions to identify hydrogeochemical characteristics of karst groundwater in Xide country, Sichuan Province. Carbonates Evaporites 1–12. doi:10.1007/s13146-017-0333-x

Zhang J, Quay PD, Wilbur DO (1995) Carbon isotope fractionation during gas-Wate exchange and dissolution of CO_2. Geochim Cosmochim Acta 59(1):107–114

Zhao M, Liu Z, Li H-C, Zeng C, Yang R, Chen B, Yan H (2015) Response of dissolved inorganic carbon (DIC) and $\delta^{13}C_{DIC}$ to changes in climate and land cover in SW China karst catchments. Geochim Cosmochim Acta 165:123–136